AIP Advances

Iron oxide–Si nanoparticle magnetic core–shell induced by the interaction of d-orbitals of Fe^{2+} with reconstructed Si dimer-like defects

Cite as: AIP Advances **10**, 055221 (2020); https://doi.org/10.1063/1.5144880
Submitted: 11 January 2020 . Accepted: 19 April 2020 . Published Online: 20 May 2020

Noha Elhalawany, Kevin Mantey, Tuan Hoang, Ersin Bahceci, Jiacheng Xu, Hakan Ates, Dmitry Gorin, Zain Yamani, and Munir H. Nayfeh

COLLECTIONS

Paper published as part of the special topic on Chemical Physics, Energy, Fluids and Plasmas, Materials Science and Mathematical Physics

View Online Export Citation CrossMark

ARTICLES YOU MAY BE INTERESTED IN

Proximal probe-like nano structuring in metal-assisted etching of silicon
AIP Advances **9**, 055228 (2019); https://doi.org/10.1063/1.5096659

Wet non-thermal integration of nano binary silicon-gold system with strong plasmonic and luminescent characteristics
AIP Advances **9**, 095039 (2019); https://doi.org/10.1063/1.5121153

Heat and mass transfer together with hybrid nanofluid flow over a rotating disk
AIP Advances **10**, 055317 (2020); https://doi.org/10.1063/5.0010181

AIP Advances
Fluids and Plasmas Collection
READ NOW

AIP Publishing

© 2020 Author(s).

Iron oxide–Si nanoparticle magnetic core–shell induced by the interaction of d-orbitals of Fe^{2+} with reconstructed Si dimer-like defects

Cite as: AIP Advances 10, 055221 (2020); doi: 10.1063/1.5144880
Submitted: 11 January 2020 • Accepted: 19 April 2020 •
Published Online: 20 May 2020

View Online Export Citation CrossMark

Noha Elhalawany,[1] Kevin Mantey,[2] Tuan Hoang,[2] Ersin Bahceci,[3] Jiacheng Xu,[4] Hakan Ates,[5] Dmitry Gorin,[6] Zain Yamani,[7] and Munir H. Nayfeh[1,a)]

AFFILIATIONS

[1]Polymers and Pigments Department, National Research Center, 12622 Cairo, Egypt
[2]Department of Physics, University of Illinois at Urbana-Champaign, Urbana, Illinois 61801, USA
[3]Department of Metallurgical and Materials Engineering, Iskenderun Technical University, 31200 Hatay, Turkey
[4]Department of Physics, University of California Davis, Davis, California 95616, USA
[5]Department of Metallurgical and Materials Engineering, Gazi University, 06500 Ankara, Turkey
[6]The Skoltech Center of Photonics and Quantum Materials (CPQM), Skolkovo Institute of Science and Technology, 121205 Moscow, Russia
[7]Department of Physics, King Fahd University, Dhahran 34463, Saudi Arabia

[a)]**Author to whom correspondence should be addressed:** m-nayfeh@illinois.edu

ABSTRACT

Redox-type charge exchange between Si nanoparticles and aqueous metal ions m^{x+} was recently used to synthesize core–shell nanocomposites in which their functionalities have been integrated. The process requires the electron (hole) affinities of the two to be different, with the efficiency of the charge exchange being strongly dependent on their difference. In this paper, we examine the interaction of Fe ions and red luminescent Si nanoparticles where the metal ion has comparable electron affinity to that of the Si nanoparticle. Scanning electron microscopy and fluorescent spectroscopy imaging show the formation of red luminescent core-shell clusters ranging from 100 nm to 500 nm. A permanent magnet is found to pull the structures indicating the formation of a magnetic phase. We use first principle atomistic computations at the unrestricted Hartree–Fock-DFT (density functional theory) level to obtain the charging energies and affinities of various ions of Fe and the Si nanoparticle. The computations indicate that Fe^{2+} cannot be oxidized to Fe^{3+} by the nanoparticle and it cannot strip one or two electrons from the nanoparticle and freely separate, resulting in bound complexes. Our analysis shows that a magnetic phase of iron oxide results from charge delocalization over the complex and a simultaneous interaction of the iron d-orbitals with the oxygen's lone electrons and the nanoparticle's reconstruction dimer-like defects. The core-shell integration at the nanoscale affords double functionality of luminescence and magnetism enhancing sensing, tracking, and delivery and enabling a variety of applications, including controlled drug delivery, underground oil and water exploration, and recovery.

© 2020 Author(s). All article content, except where otherwise noted, is licensed under a Creative Commons Attribution (CC BY) license (http://creativecommons.org/licenses/by/4.0/). https://doi.org/10.1063/1.5144880

INTRODUCTION

Charge exchange has been widely known in the context of collisions between a singly or multiply charged ion and an atom. In such collisions, a reduction–oxidation (Redox) electron capture may occur.[1] Recently, the charge exchange process has been applied to nanoparticle–ion collisions, a system involving multiple atoms, with the aim of integration of different materials and functionalities. In this case, a redox charge (electron or hole) transfer takes place provided the electron affinities of the ion and the nanoparticle

© Author(s) 2020

are significantly different.[2,3] In specific, the collisions of silicon nanoparticles and metal ions m^{x+} have attracted great interest[4–6] because of potential to produce composite structures with a silicon nanoparticle core and a metal-based shell.[7–9] In this nano core-shell configuration, the luminescence functionality of the nanoparticles is integrated with that of a metal (or a metal-based material). For example, using erbium, magnesium, and gold metals, infrared[7] and visible fluorescence[8] and plasmonic[9] functionalities were integrated, respectively, with the Si nanoparticle luminescence.

Another metal of interest for charge exchange with silicon nanoparticles is the metal iron, which has the potential to integrate luminescence with magnetism. Magnetic nanoparticles have been offering great potential in a variety of applications, including magnetic energy storage, information storage and spintronic, magnetic fluids, catalysts, and biomedicine.[10,11] The importance to biomedicine stems from the fact that the magnetic material can be directed with a magnetic field, which enables smart drug delivery and enhances medical imaging. Ferrite nanoparticles, based on iron oxide compounds, such as ferromagnetic (Fe_3O_4) and maghemite (γ-Fe_2O_3) are the most explored for biomedical applications. However, the integration of silicon and iron may not be amenable to the charge exchange process as the iron ion has an electron affinity comparable to that of silicon. In fact, the electron affinities of Fe^{2+} and hydrogen-terminated silicon are nearly equal, being −0.45 and −0.43, respectively.[12] Even if a redox type reaction proceeds for this system, the process may result in two separated free charged species without integration. Moreover, it is not clear if the interaction would fully reduce (neutralize) the ion and deposit the metal as well as allow a follow-up oxidation process to produce the magnetic oxide phase. In addition, it is not clear if the polarizability of silicon nanoparticles compares well to that of the water solvent to allow joint binding to the ion to form a stable hydrated silicon nanoparticle–ion charged complex.

In this paper, we examine experimentally and theoretically, the charge exchange process for the comparable affinity case of the iron and silicon nanoparticle binary system. We monitor the optical, topographical, and magnetic characteristics of a mixture of an iron salt ($FeCl_2$) in water and Si nanoparticle colloid suspension in isopropyl alcohol. The luminescence intensity of the colloid and its spectral distribution under UV excitation as well as its optical characteristics in room light are monitored. The magnetic response of the mixture to external magnets is carried out. Thin films prepared from the colloids are imaged and analyzed for material composition and size distribution by scanning electron microscopy (SEM) and energy dispersive x-ray spectroscopy (EDS) to check for integrated architectures (for example core–shell nanostructures). To evaluate the conditions for redox charge exchange processes, we carry out, at the UHF-DFT level, first principle atomistic calculations of the charging energies and electron affinities of various ions of the nanoparticle and the Fe ions as well as the energy potential surfaces with the interparticle–ion distance and the binding energy of different complexes of the binary system.[13] We also calculate the effect of the solvent (water) medium polarization screening as well as the interaction of the lone electron pairs of solvent oxygen with the iron d-orbitals (weak "dangling bonds" of unfilled orbitals) on the binding and stability of the complex. The calculations point to the formation of a bound (0.49 eV binding) charged complex (hydride Sinp–Fe)$^{2+}$ with no charge exchange, rather than its total charge delocalized over the entire complex. Strong d-orbitals interaction with the lone electrons in the water oxygen allows for the subsequent formation of "Sinp–Fe_2O_3" composite structures, integrating the magnetic iron oxide with the luminescent silicon nanoparticle core, providing optical, luminescence, and magnetic functionality.

EXPERIMENTAL

The nanoparticles are prepared from Si wafers by chemical etching in HF/H_2O_2 using an electric field or a hexachloroplatinic acid catalyst.[14] Generally, we produce a set of H-terminated silicon nanoparticles with discrete size Si_nH_x particles of 1.0 ($Si_{29}H_{24}$), 1.67 (Si_{123}), 2.15, and 3.0-nm diameter with confinement bandgaps of 3.44 eV, 2.65 eV, 2.39 eV, and 2.2 eV.[15] The particles have hydrogenated reconstructed surfaces consisting of a network of bulk-like (2 × 1) reconstruction Si–Si dimers on (001) facets.[16] Quantum Monte Carlo (QMC) calculations,[17] which employ Hartree–Fock pseudopotentials, confirm the movement of the surface Si atoms (0.75 Å each) from the next nearest spacing of 5.4 Å to the tetrahedral spacing of 2.36 Å reconstructing to form dimer-like H–Si–Si–H. Those dimers have been known to behave as non-bulk intrinsic silicon-based defects.[18] The 3-nm can be easily seen using a transmission electron microscope (TEM) resolving the atomic planes. Aqueous ions of iron Fe^{2+} and Fe^{3+} were prepared by dissolving certain amounts of iron salts ferrous chloride ($FeCl_2$) and ferric chloride ($FeCl_3$), respectively, in deionized water. Absorbance measurements were recorded with a Varian Cary 5 G spectrophotometer. The magnetic response of the structures in solution was examined using a stack of permanent magnets. A set of eight neodymium–iron–boron (NdFeB) permanent magnets are set into a configuration, in which we stack 8 of them on top of each other which produces a dipole field.

Thin films of the structures were prepared by drop-drying under ambient conditions on a device-quality silicon wafer. Thin films were also prepared by propelling the solution using a conducting stainless biased nozzle. The topography of the films was imaged and observed by scanning electron microscopy (SEM) in a back scattering mode, and the material is analyzed by energy dispersive x-ray spectroscopy (EDS or EDX), which is a chemical microanalysis technique used in conjunction with scanning electron microscopy (SEM). The intensity and spectral distribution of photoluminescence of the solutions as well as of the films in the range of 350 nm–800 nm were monitored using a holographic grating in association with a fiber optic system that collects the luminescence.

The theoretical analysis and calculations of the charging energies of $Si_{29}H_{24}$ and Fe were done at the UHF-DFT level using the B3LYP functional with the TURBOMOLE quantum computational package. We use the conductor-like screening model (COSMO) to calculate and analyze the electrostatic interaction of the Fe ion and the nanoparticles with the water solvent.

RESULTS

Solutions of salts were prepared for absorption measurements. We prepared 1.1 mM solutions of ferrous chloride ($FeCl_2$) and

© Author(s) 2020

ferric chloride ($FeCl_3$) by adding the corresponding salt to de-ionized water. Samples were placed in a fused quartz cuvette, and the absorbance measurements were recorded with a Varian Cary 5 G spectrophotometer. After the absorbance of an iron solution was measured, it was mixed in the ratio 9:1 with the stock silicon nanoparticles in isopropyl alcohol (10 μM) and the absorbance of the resulting mixture was measured. A solution containing 9:1 de-ionized water to nanoparticle solution was also prepared to provide a solution with the same amount of water and silicon nanoparticle solution as the previous mixture. While the proposed structure of the nanoparticles is non-polar, the 9:1 mixture of water and isopropanol resulted in no precipitation and appeared stable. Water was chosen to be the predominant solvent for the ease in obtaining solutions of metallic ions. The iron chlorides separate into iron and chloride ions with solvation shells in water[19] because iron interactions with isopropanol are comparatively weak requiring strong anhydrous conditions for isopropanol coordination with iron.[20]

Absorption measurements

The background absorption was corrected for dark counts and the spectra from a cuvette with de-ionized water was subtracted as a blank. The result is shown in Fig. 1. The concentrations of silicon nanoparticles are the same in the three solutions containing them. The dilute silicon nanoparticles absorb very little [Fig. 1(e)], although features at 225 nm and 275 nm can still be seen. These correspond to the 4.5 eV and 5.5 eV peaks seen in the measurements previously reported using more concentrated samples.[21] The $FeCl_2$ solution containing Fe^{+2} ions is relatively featureless in this range [Fig. 1(d)], while the $FeCl_3$ (Fe^{+3} ions) absorbs strongly with a broad peak at 290 nm [Fig. 1(a)]. For both ions, mixing with the silicon nanoparticle solution significantly affects the absorption spectra [Figs. 1(b) and 1(c)]. Neither ion nor particle mixture is a linear combination of the absorbance of the parts indicating a strong interaction and possibly the formation of a charged complex. Furthermore, the features of both mixtures are same. As the wavelength decreases, the absorbance slowly increases until about 270 nm where a bend occurs in the spectra with a faster increase in absorbance at lower wavelengths. This may indicate that the resulting structures are similar in each case.

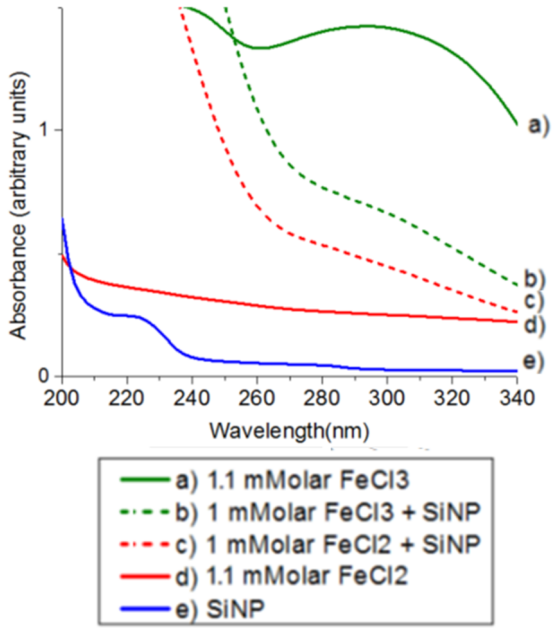


FIG. 1. Absorbance of mixtures of Fe^{2+}/Fe^{3+} and silicon nanoparticles placed in a fused quartz cuvette and recorded with a spectrophotometer in the range 200 nm–340 nm. (a) (solid green) 1.1 mM $FeCl_3$, (b) (dotted green) 1 mM $FeCl_3$ + Si nanoparticles, (c) (dotted red) 1 mM $FeCl_2$ + Si nanoparticles, (d) (solid red) 1.1 mM $FeCl_2$ and (e) (solid blue) Si nanoparticles. The $FeCl_2$ solution containing Fe^{2+} ions is relatively featureless in this range, while $FeCl_3$ (Fe^{+3} ions) absorbs strongly with a broad peak at 290 nm. Neither ion nor particle mixture is a linear combination of the absorbance of the parts.

Luminescence

We then monitored the photoluminescence of mixtures of Fe ions with silicon nanoparticles. Particle solutions are prepared by dissolving the nanoparticles in an appropriate solvent, such as isopropyl alcohol (IPA). We use a salt of iron to provide the metal ions of Fe^{2+} in water. Si nanoparticle colloid in isopropyl alcohol (10 μM) is added to 0.5 ml of 1.65×10^{-3} M of $FeCl_2$–water solution while monitoring the luminescence intensity and the spectral distribution. The mixture is then homogenized for 15 min using a 1 cm bore homogenizer at a speed of 16 000 rpm. For the long-term storage and to avoid further reactions with the excess reactants, the samples were centrifuged and the clusters were recovered. They were re-dissolved in isopropyl alcohol.

The reaction shows in room light brown/orange color, as shown in Fig. 2(a). We show in Fig. 2(b) and the inset the development of luminescence from the sample with time under UV irradiation. The colloid is observed to give orange/red luminescence; however, with time, we observe some precipitation as well as some quenching in the luminescence. Figures 2(c) and 2(d) give the luminescence spectrum taken before and after mixing the reagents, respectively, using holographic grating and a CCD detector; the spectra show a luminescence band over 550 nm–750 nm.

We placed a stack of permanent magnets to the side of a glass container. A set of eight neodymium–iron–boron (NdFeB) permanent magnets are set into a configuration in which we stack 8 of them on top of each other which produces a dipole field. With the time on the order of minutes, the material gets pulled by the magnet and gets pinned down at the inner wall, as shown in Fig. 3(a). Upon irradiation with UV light, the drawn material shows red luminescence, as shown in Fig. 3(b).

We dispensed some of the material on a Si wafer using drop evaporation (casting), dried them under ambient conditions, and observed them with a scanning electron microscope in a back scattering mode. Figure 4 shows that the material consists of spherical particles of a diameter in the range of 100 nm–400 nm. The variance points to a process in which clusters of the Si particles act as nucleation sites that form spherical structures. Figure 4 shows that there is a good fraction of the clusters that appears to consist of a dark core, associated with a Si core, surrounded by a lighter shell, associated with iron. The Si core is estimated to be 20 nm in diameter,

© Author(s) 2020

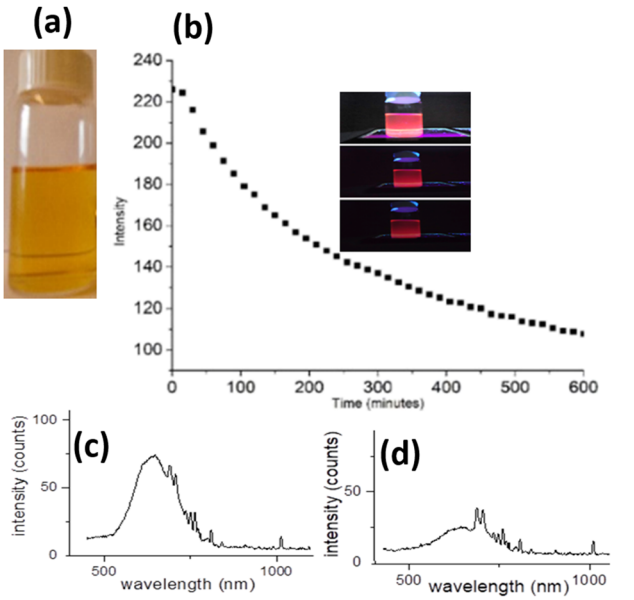


FIG. 2. Mixture of Fe^{2+} and silicon nanoparticles (a) in room light showing brown/orange color. (b) The peak intensity of the luminescence at a point near the top of bottle with time under UV irradiation. Inset Three photoluminescent photos of a sample taken at consecutive time (from top to bottom) showing the progress of precipitation and some quenching. The luminescence spectrum taken using holographic grating and a CCD detector (c) before and (d) after mixing the nanoparticles with the iron salt.

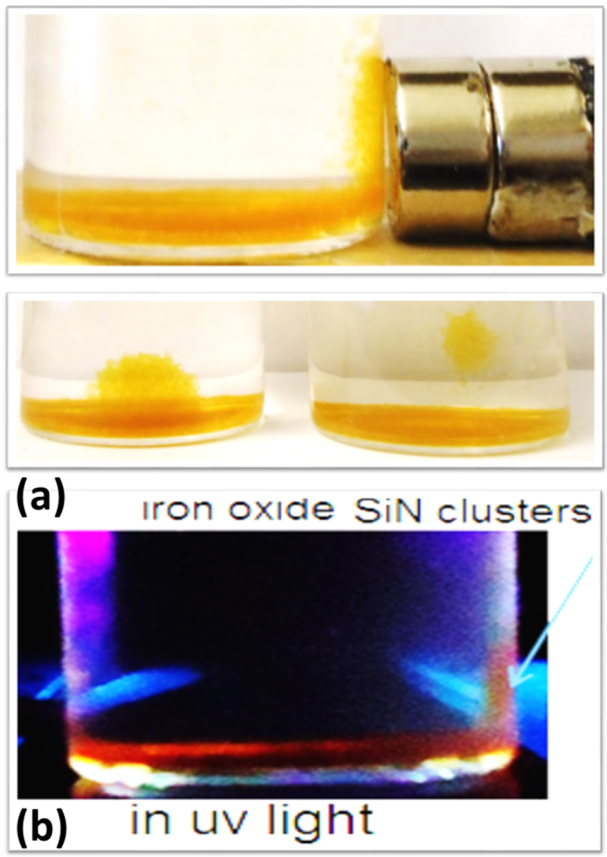


FIG. 3. Effect of an external magnet on the colloid. A stack of permanent magnets placed to the side of a glass container. With time on the order of minutes, the material gets pulled by the magnet and gets pinned down at the wall (a) imaged in room light and (b) imaged under irradiation by UV light, where the drawn material shows red luminescence.

corresponding to a Si nanoparticle cluster of 100 nanoparticles (each of a diameter of 2.9 nm).

Stability propulsion measurements

To examine the charging and stability of the structures, we propelled the structures via an electric field. Particle solution is placed in a reservoir that feeds into a conducting stainless biased nozzle.[22–27] A grounded conducting plate is placed at a distance of ~3 cm from the opening of the nozzle [see Fig. 5(a)]. The nozzle is electrically biased with respect to the ground plate, which establishes a non-uniform electric field between them. A target substrate (typically a silicon wafer) is placed in front of the grounded plate to collect the particles. At a positive threshold voltage bias of 2.26 kV with respect to the counter grounded conducting plate, the colloid is propelled and the material gets pinned down on the substrate, resulting in the formation of a thin film. This indicates that the structures get charged in the process. The image in room light of the substrate shows a gray stain film shown in Fig. 5(b). A line profile through the gray scale image showing a stronger stain on a central disc is shown in Fig. 5(c). Figure 5(d) shows a photo of the film on exposure to UV radiation at a wavelength of 254 nm; it shows that the film is luminescent, observable by the naked eye. The corresponding luminescence spectrum of the deposited film (not shown) displays the characteristic red luminescence of the Si nanoparticles. A closer look would show that the luminescent image has a similar line profile to the gray stain

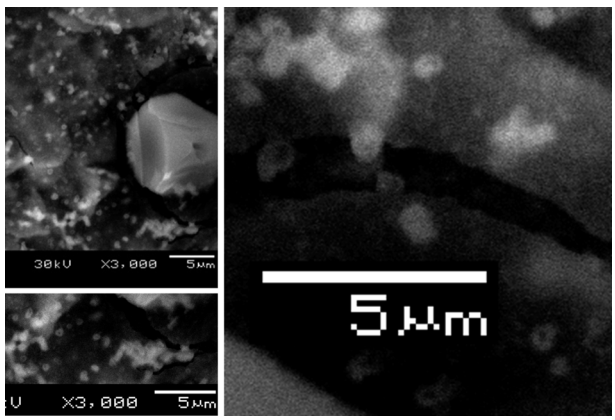


FIG. 4. Scanning electron microscope imaging of the core-shell. A good fraction of the clusters appear to consist of a dark core, associated with a Si core, surrounded by a lighter shell, associated with iron-based material. The Si core is estimated to be 20 nm in diameter corresponding to a Si nanoparticle cluster of 100 nanoparticles (each of a diameter of 2.9 nm).

© Author(s) 2020

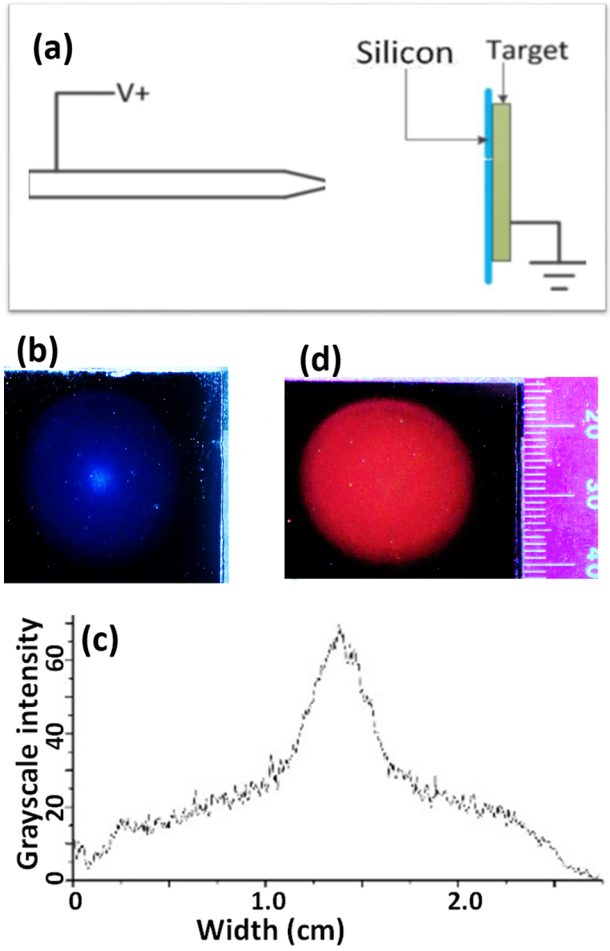


FIG. 5. Electrospray of a thin film of the colloid of the Fe^{2+}–silicon nanoparticles. (a) Layout of the spray setup. (b) The gray image in room light of the film. (c) A line profile through the gray scale image. (d) The corresponding luminescent image of the film under exposure to UV radiation at a wavelength of 254 nm.

indicating more intense deposition over an inner disc. The gray stain is related to the effect of ions landing on the substrate at a high speed due to electric field acceleration.

Controlled samples of Si nanoparticles in isopropyl alcohol without mixing with the Fe ions were also propelled toward a substrate on which they were deposited.[28,29] The particles are found on the substrate exhibiting their characteristic luminescence. However, the propulsion occurs for both positive and negative bias with respect to the grounded plate; in the case of the mixture of particles and ions, propulsion is found to occur only for positive bias. When the biasing is reversed from positive to negative, we find the insignificant deposition of silicon nanoparticles, while the nozzle becomes readily clogged. This is consistent with the fact that the ions act as a carrier (complexing) of the nanoparticles and that there are insignificant amounts of unreacted nanoparticles with the positive ions.

THEORETICAL

The underlying principle of the interaction of the ions with silicon is charge exchange.[30] First, in the collision, the iron ions are attracted to silicon nanoparticles by electrostatic polarization forces. The interaction between them at a close distance may result in a redox type reaction resulting in two free charged species. The accuracy of the procedure and calculation methods are checked against the correct iron ionizations and solvation energies, which are known in the literature.

The 3-nm particle is too big for atomistic first principle simulations and computations; therefore, we use as a model for illustration, in which there is a smaller 1-nm particle consisting of 29 silicon atoms and 24 hydrogen atoms, which is manageable by such simulations. The calculations of the charging energies of $Si_{29}H_{24}$ and Fe were done at the UHF-DFT level using the B3LYP functional with the TURBOMOLE quantum computational package.[31] The TZVP basis was used, which is a triple split valence basis with polarization functions added for each atom.[32–34] The energy of the species in water was obtained with the COSMO method of approximating the particles embedded in a continuum dielectric of $\varepsilon = 78.4$ and using a solvent radius of 1.3 Å.

Dimer defect

The 1 nm silicon nanoparticle $Si_{29}H_{24}$ has no terminations on its surface with lone electron pairs, such as an oxide or nitrogen group, which are commonly found in the ligands of a charged complex. However, the surface reconstruction dimers pull to open up 4 hexagonal rings on the surface[16,17] affording an alternative mechanism. For example, a ferrous ion may sit within one of these rings reducing the energy by effectively spreading the charge over a larger volume represented by the silicon nanoparticle. If the particle can act as an "effective polarizable medium" better than the water, the charged complex may then be stable.

Continuum and complex solvation model (COSMO) (water–iron)

In this section, we calculate the energies of the silicon particle and the iron atom at various charging energies in an aqueous environment. We use the conductor-like screening model (COSMO)[35,36] to calculate and analyze the electrostatic interaction of the Fe ion and the nanoparticles with the water solvent. We first present the possible model approximations for the water solvent. Water is divided into two regions: an inner-cluster of water and an external/outer continuum of water, with the total model being a combined sum of the two. In the first inner-cluster part, the interactions between the lone electrons in oxygen and the d-orbitals of the ions (totaling 6 orbitals) are accounted for explicitly as a gas phase model and are expected to play a major role. For instance, the gas phase structure for ferrous iron (Fe^{2+}) and 6 water molecules gives a hexa-aqua complex (solvation shell), as illustrated in Fig. 6. The oxygens attach as ligands in a cubic structure. The solvation shell is not made of strong covalent bonds, and the water molecules still rearrange with inner solvation shell exchanges occurring on a time scale of about 10 ns for Fe^{2+} ions.[19] At this short distance of the inner cluster, the lone pairs of the oxygen in water will interact with the unfilled

© Author(s) 2020

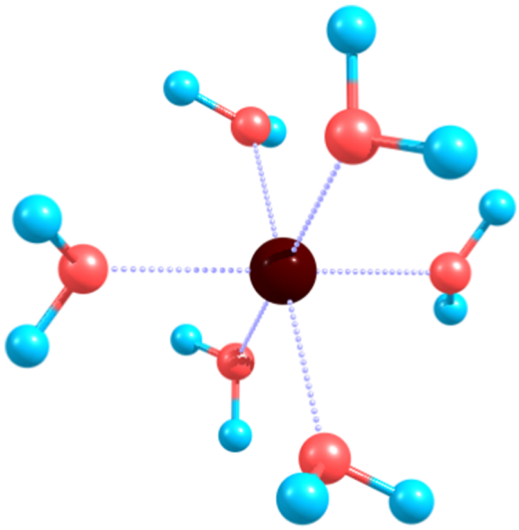


FIG. 6. The gas phase hexa-aqua complex structure for ferrous iron (Fe^{2+}) and 6 water molecules. Hydrogen in blue. Oxygen in red. Fe ion in black. The oxygen attach as ligands in a cubic structure.

orbitals (weak "dangling bonds") of iron to form a complex with water.

Beyond the inner cluster, we have the continuum water component, which does not include the oxygen d-orbital. The model accounts for water interactions in terms of dielectric screening. In this region, water molecules move sufficiently randomly enough about the ion allowing for a continuum average approximation to be appropriate. Clearly, the water molecules far from the ion are uncorrelated with the iron atom and therefore fit the approximation well. Higher order and weaker solvation shells of water form around this inner solvation complex due to the hydrogen bonding with the inner shell water molecules. While including the higher order complexes leads to some improvement, a combined first inner-cluster and an external continuum model for water has been found to account for the vast majority of the complex shell interaction.

In order to remain consistent for comparison, six water molecules were used for the solvation of each of the four iron atom charges considered here (Fe^0, Fe^{1+}, Fe^{2+}, and Fe^{3+}). The solvation energy was calculated from the change in energy of the reaction

$$Fe^{X+}(gas) + 6H_2O(solv) \rightarrow [Fe(H_2O)]^{X+}(solv),$$

where the solvent phase energy of a single water molecule was found to be −76.43816 Hartree (and a gas phase/vacuum energy of −76.42592 Hartree). The resulting solvation energies are within 3% of the experimental values therefore bringing the calculation accuracy to the same level as the ionization energies in vacuum showing the accuracy of this method.

Charging energies of the nanoparticles and the ions

The energy of the silicon particle and iron atom in vacuum (or "gas phase") at various charging energies is given in Table I. The

TABLE I. Energy of the silicon particle and iron atom in vacuum for various charging states.

1 nm silicon nanoparticle $Si_{29}H_{24}$		
Charge	Unpaired electrons	eV (relative to neutral)
−1	1	−1.462
0	0	0
+1	1	7.292
+2	0	16.662
	2	16.658
Iron atom		
Energy relative to neutral atom		
		Calculated (eV)
Fe (+1)		7.725
Fe (+2)		24.311
Fe (+3)		55.708

electronic density used for the density functional calculations is built from an unrestricted Hartree–Fock (UHF) type slater determinant, which cannot correctly handle the degeneracy of the iron orbitals. Instead of the electrons being shared equally between the 5d atomic orbitals, the electrons are placed in the first unfilled shell.

We plot, for convenient display in Fig. 7, selected vacuum ionization energies (from Table I) in an energy level diagram format. The energies for the iron atom are given on the left and those for the silicon nanoparticle are given on the right of Fig. 7. The silicon particle ionization energy and electron affinity are found to be 7.29 eV and 1.46 eV, respectively. This is much closer to the atomic values of the silicon atom (8.15 eV and 1.38 eV, respectively) than to the crystalline bulk silicon values of 4.05 eV and 5.17 eV. This further demonstrates that the silicon nanoparticle is most appropriately discussed in the molecular regime than the approximations from the

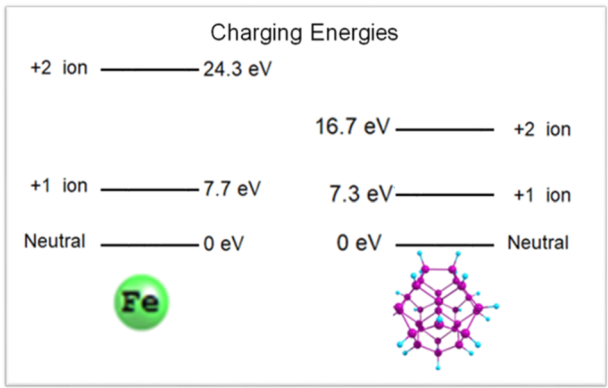


FIG. 7. A plot of selected charging ionization energies of an ion atom and a silicon nanoparticle (given in Table I) in an energy level diagram format. (Left) Fe atom and (right) silicon nanoparticle.

© Author(s) 2020

TABLE II. Energy of the silicon particle and iron atom in vacuum for various charging states.

1 nm silicon nanoparticle $Si_{29}H_{24}$ in water		
Charge	Unpaired electrons	eV (relative to neutral)
−1	1	−2.314
0	0	0
+1	1	5.475
+2	0	11.232
	2	11.228
Iron solvation energy in water		
		Calculated (eV)
Fe (+1)		4.536
Fe (+2)		12.734
Fe (+3)		28.643

crystalline condensed matter regime. The energy of the silicon particle and iron atom in water at various charging energies is given in Table II.

Potential energy surface of the bound complex using the continuum model

Structures were first calculated at the UHF-DFT level with a TZVP basis set and the B3LYP functional using the TURBOMOLE quantum computational package.[31] The first structures were calculated without solvation models to investigate if the polarization of the silicon particle was sufficient for reduction in energy to prevent each species to just become singly charged and separate due to Coulomb repulsion.

Initial attempts at placing the iron atom above the hexagonal silicon ring resulted in the iron atom falling below the ring into the particle interior during relaxation. A local minimum energy structure was found. This "interior" minimum was calculated for 0, 2, 4, and 6 unpaired electrons and found to exist in each case. The lowest energy structure contained 4 unpaired electrons, and $\langle S^2 \rangle$ = 6.066 showing low spin contamination. Both Mulliken and Loewdin population analyses gave 3 unpaired electrons in the iron d-orbitals and none in the s- and p-orbitals. Considering the electronic configuration predictions of Fe^{1+}, this is in agreement with one charge transferred between the Si nanoparticle and the initial ferrous ion, leaving each singly charged.

Vacuum calculations

The energy of the complex in vacuum as a function of the distance of iron from the center of the silicon nanoparticle (the center nuclei) was calculated for this structure (shown in Fig. 8—solid curve). In the simulation, the ion approaches the nanoparticle from a distance far from a state of Fe^{1+} ion and a singly charged nanoparticle, where the total energy is taken zero. Outside the silicon nanoparticle, an energy minimum is found at a distance of

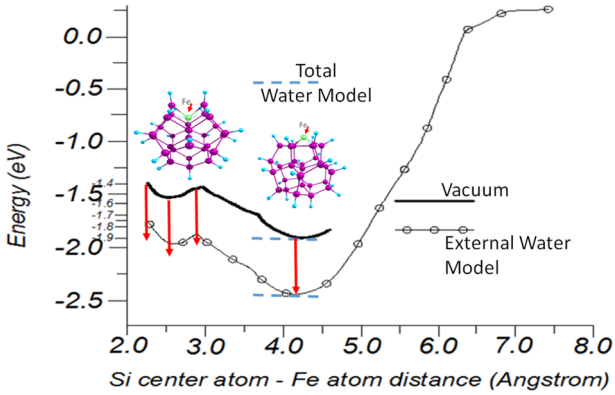


FIG. 8. Calculated potential energy surface of an Fe^{2+} ion and a silicon nanoparticle showing the energy of the complex as a function of the distance of iron from the center of the silicon nanoparticle (the center nuclei) for this structure. At each distance, the structure was relaxed in the 4 unpaired electron configuration in vacuum (solid curve) and gas phase (circle-solid) in water liquid using the continuum water model. (Left inset) The Fe–silicon nanoparticle prototype model for the Fe inside the particle. (Right inset) The Fe–silicon nanoparticle prototype model for Fe outside the particle. We display a finer energy scale between −2 eV and −1.5 eV on the vertical scale for easier reading.

4.15 Å from the center of the particle. In this molecular prototype configuration, the Fe atom rests on top of the hexagonal silicon ring, as shown in the right inset in Fig. 8. With further calculations, the ion may enter inside through the hexagonal ring of the particle where it faces a barrier at a distance of 3 Å from the center of the particle, after which it enters into a second local minimum at 2.55 Å, as shown in the left inset in Fig. 8. The minimum of the well outside minimum is 0.43 eV below the barrier through the ring and 1.90 eV below the energy of a distantly separated Fe^{1+} ion and a singly charged nanoparticle, as calculated from the previously obtained ion energies. At each distance, the structure was relaxed in the 4 unpaired electron configuration. The inner local minimum was found to be a 0.09 eV deep well from the top of a transition point of the barrier when moving through the hexagonal ring. Thus, it is easier for the system to form the complex where the ion is outside the particle than when the ion is inside the particle. It takes an energy of more than 0.4 eV to overcome the barrier at the entry point in the particle, i.e., entering the hexagonal silicon ring. If the ion is already inside, it takes only 0.9 eV of energy to come out of the particle.

Aqueous calculations

The continuum part of the approximation COSMO solvation model was first used to calculate how the dielectric screening energy of water affects the vacuum potential energy surface. The result is shown in Fig. 8—solid-circle. The calculations show stronger binding energies for all distances (potential surface shifts down); the shift, however, is not uniform with the distance as the vertical arrows display. The presence of water causes the inner equilibrium minimum to become shallower, with the barrier for entering the hexagonal ring dropping to a lower value (0.07 eV above the inner minimum). The

© Author(s) 2020

outer minimum is 0.57 eV below the barrier through the ring, and 2.45 eV below the long distance limit of an Fe^{1+} ion and a single charged nanoparticle in water. It is to be noted that near the outer minimum, the structure was allowed to relax for a configuration with 2 unpaired electrons and 4 unpaired electrons. The 4-electron case was the minimum energy, consistent with the silicon particle and iron atom each having a single charge and remaining spin aligned.

Complex (Si–Water–Fe) prototype

We now use the total water model in the atomistic calculations. The model is the combination of the first inner-cluster and the external continuum. This is an improved approximation, which allows us to obtain more accurate binding energy of this complex than the calculations given in Fig. 8 obtained in vacuum or with the external continuum model for water. The prototype given in Fig. 9 is the proposed charge complex in the total model. A computational study of this prototype and its variation was carried out to optimize the prototype. The number of water molecules in the first inner-cluster in the prototype was varied around 3. In this level of computation, we include the interaction of lone pairs of the oxygen present in water molecules as well as the dimer-like defects in the Si particle with the unfilled d-orbitals (weak "dangling bonds") of iron simultaneously. The computations showed that to form a complex with the nanoparticle and water, the iron will not have a full hexa-aqua shell as in the free Fe^{2+} case (see Fig. 6). We experimented with the number of water molecules in the first solvation shell. The computation shows that when in the equilibrium position above the hexagonal silicon ring, roughly half of the iron atom is obscured from direct interaction with the solvent. So the silicon nanoparticle must replace 3 of the 6 water molecules in the iron solvation shell. This number turned out to be the most likely scenario.

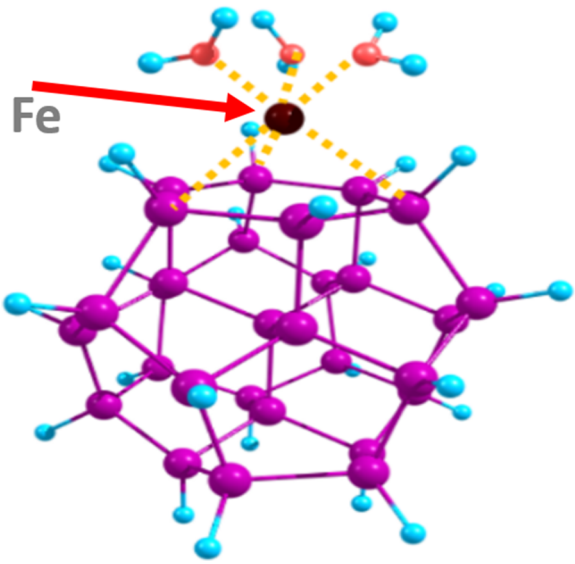


FIG. 9. Complex prototype. It consists of an iron ion sandwiched between a silicon nanoparticle and a three water molecules shell. The complex binding (4.9 eV) via interactions with three d-orbitals of the ion with a silicon nanoparticle and three d-orbitals of the ion with three water molecules.

The resulting structure, shown in Fig. 9, was allowed to relax and the total binding energy was evaluated by considering the dissociation reaction

$$\left[(Si_{29}H_{24})Fe(H_2O)_3\right]^{+2} + 3H_2O \rightarrow \left[Fe(H_2O)_6\right]^{+1} + \left[Si_{29}H_{24}\right]^{+1},$$

where all energies used the COSMO solvation model. The binding energy was found to decrease from 1.9 eV in vacuum to 0.49 eV in the presence of water. This shows that d-orbital interactions with water softened the binding energy, but the proposed complex is still found to be stable against dissociation in water despite the Coulomb repulsion due to each species being charged. The horizontal dotted lines at −1.9 eV, −2.5 eV, and −0.49 eV in Fig. 8 label the binding levels in the vacuum environment, water continuum model, and the total water model with d-orbital interactions. Marking the binding energy (at 0.49 eV) of the complex in Fig. 8 serves as a convenient comparison with the binding energies under other approximation.

DISCUSSION

Magnetic phase

In the proposed complex, (i) the charge is delocalized over the entire complex of 4-nm diameter and (ii) the d-orbitals of Fe^{2+} interact with both the Si nanoparticle and the oxygen molecules in water. The proximity of oxygen to Fe allows the oxidation of iron and the formation and deposition of iron oxide in its magnetic phase on the silicon nanoparticle (or a cluster of silicon nanoparticles). Thus, the emergence of the magnetic phase supports the formation of the complex as an intermediate stage (Fig. 3). Since the calculations indicate that the complex either in the continuum or in the total model is bound, they support the idea that the particle acts as an "effective polarizable medium" better than the water, allowing the charge complex to be stable. The ion is sandwiched between the nanoparticle and the water molecules.

We should note that the sensitivity offered by magnetic particles can be enhanced further by the clustering of a number of individual superparamagnetic nanoparticles into clusters to form magnetic beads. We should also note that there are other magnetic materials of interest with a high magnetic moment, such as cobalt and nickel. The major advantage of iron over these materials is the possibility for *in vivo* applications.[11] Cobalt and nickel metals can cause oxidative stress or long-term changes in enzyme kinetics.

Electric features

The process of charge exchange has been widely known for a long time but between ions and atoms. With the emergence of nanoscience, the collision between ions and nanoparticles opened up wide applications. In this process, the electron capture in slow collisions between multiply charged ions I^{p+} and an atom A (or nanoparticle) occurs through a pseudo-crossing of the adiabatic potential energy curves of the combined molecule or cluster AI^{p+}. The presence of a Coulomb repulsion between the collision partners after the collision ($I^{(p-1)+}$–A^{+}) is the basic reason for the existence of such pseudo-crossings at large distances. The present system of silicon

© Author(s) 2020

nanoparticle–iron ion is unique since the partners have nearly equal electron/hole affinities, which renders charge exchange processes weak and not plausible. For this particular situation, the study ruled out an interaction between them at a close distance that results in a redox type reaction resulting in two free charged species. It also ruled out that the charge is transferred between them and that it ruled out even if a charge complex is formed. Moreover, the calculated charging energies indicate that a ferrous Fe^{2+} ion cannot be oxidized to Fe^{3+} by the silicon nanoparticle in water due to energy constraints. Furthermore, an Fe^{2+} ion cannot strip one or two electrons from a silicon nanoparticle in water and then freely separate. Therefore, without additional energy supplied externally, the ion energies restrict the interactions to those resulting in bound complexes.

The study showed that the oxidation state of the metallic atom remained a useful quantity when discussing charged complexes since the energies of various ions of the nanoparticles in solution compared to the iron ions was helpful in narrowing the range of possible interactions. This was also consistent with the fact that the bonds in a solvation complex in a water medium are much more ionic than covalent in nature and with the fact that the ligand bonds are usually longer than ordinary single covalent bonds.

As to the mechanism for the interaction with Fe^{2+}, silicon nanoparticle has no terminations on its surface with lone electron pairs, such as in oxygen (or nitrogen group), which are commonly found in the ligands of a charged complex. This is unlike the interaction of Fe^{2+} with water, which proceeds through the interaction between lone electrons in oxygen and the d-orbitals of the ion. The calculations and the experimental findings showed that the surface reconstruction dimer-type defects on the nanoparticles serve as a nontraditional alternative ligand for the interaction with the ions. Reconstruction open up 4 hexagonal rings on the surface, and a ferrous ion may sit within one of these rings reducing the energy by effectively spreading the charge over a larger volume represented by the silicon nanoparticle. The particle can act as an "effective polarizable medium" better than the water allowing the charged complex to be stable. The above calculations and simulations, indeed, confirm the role of interactions with surface reconstruction dimer-type defects.

Applications

Finally, the integration of luminescence with magnetic functionalities enables a multiplicity of synergetic application in the field of sensing, tracking, and delivery. Magnetic nanoparticles offer great potential in a variety of applications, including magnetic energy storage, information storage and spintronic, magnetic fluids, catalysts, and biomedicine.[10,11] The importance to biomedicine stems from the fact that a magnetic material can be directed with a magnetic field, which enables drug delivery and enhances medical imaging.

CONCLUSION

In conclusion, we examined the charge exchange process between the Si nanoparticles and metal ions having comparable electron affinities. We observed cluster sizes ranging from 100 nm to 500 nm in the configuration of core-shell, with a red luminescent nanoparticle cluster as a core and a shell made up of a magnetic phase of iron oxide. The structures are magnetic, as a permanent magnet placed near the colloid pulls the suspended red luminescent structures. Our first principle atomistic calculations at the UHF-DFT level confirm the formation of a hydrated bound complex with a binding of 0.49 eV. The theoretical analysis points to the effects of the delocalization of the charge over the entire complex and interactions between iron d-orbitals (weak "dangling bonds" of unfilled orbitals) and lone electron pairs of oxygen as well as the reconstructed Si dimer-like bonds. The formation of stable robust hybrid iron oxide–Si nanoparticles core-shell structures with a luminescent core and magnetic shell affords integrated optical, luminescence, and magnetic functionalities, which are useful for a wide variety of sensing, tracking, and delivery applications in biomedical and underground water and oil exploration.

REFERENCES

[1] J. B. Hasted, S. M. Iqbal, and M. M. Yousaf, J. Phys. B: At. Mol. Phys. **4**, 343 (1971).
[2] S. Süzer and Ö. Dag, Can. J. Chem. **78**, 516 (2000).
[3] R. H. Petrucci, W. S. Harwood, G. F Herring, and J. D. Madura, *General Chemistry: Principles & Modern Applications*, 9th ed. (Pearson/Prentice Hall, Upper Saddle River, New Jersey, 2007).
[4] M. H. Nayfeh, E. Rogozhina, and L. Mitas, "Silicon nanoparticles: Next generation of ultrasensitive fluorescent markers," in *Synthesis, Functionalization, and Surface Treatment of Nanoparticles*, edited by M.-I. Baratron (American Scientific Publishers, 2002).
[5] M. H. Nayfeh and L. Mitas, *Silicon Nanoparticles: New Photonic and Electronic Material at the Transition between Solid and Molecule*, Nanosilicon, edited by V. Kumar (Elsevier, 2007), p. 1.
[6] M. H. Nayfeh, *Fundamentals and Applications of Nano Silicon in Plasmonics and Fullerenes* (Elsevier Publishing, 2018).
[7] T. Hoang, N. Elhalawany, B. Enders, E. Bahceci, L. Abuhassan, and M. H. Nayfeh, Appl. Phys. Lett. **109**, 261103 (2016).
[8] A. Kocyigit, N. Elhalawany, E. Bahceci, B. Enders, K. Puthalath, L. Abuhassan, Z. Yamani, and M. Nayfeh, AIP Adv. **8**, 055324 (2018).
[9] B. Enders, A. Kocyigit, E. Bahceci, N. Elhalawany, A. Nayfeh, O. Alshammari, M. Alsalhi, and M. Nayfeh, AIP Adv. **9**(9), 095039 (2019).
[10] B. Issa, I. Obaidat, B. Albiss, and Y. Haik, Int. J. Mol. Sci. **14**, 21266 (2013).
[11] M. P. Marszałł, Pharm. Res. **28**(3), 480 (2011).
[12] P. Atkins, *Physical Chemistry*, 6th ed. (W. H. Freeman and Company, New York, 1997).
[13] K. A. Mantey, "Structure, electronic levels, and ionic interactions of 1 nanometer silicon particles," Ph.D. dissertation (University of Illinois at Urbana-Champaign, 2011); available at https://www.ideals.illinois.edu/bitstream/handle/2142/26172/Mantey_Kevin.pdf?...1by.
[14] D. Nielsen, L. Abuhassan, M. Alchihabi, A. Al-Muhanna, J. Host, and M. H. Nayfeh, J. Appl. Phys. **101**, 114302 (2007).
[15] G. Belomoin, J. Therrien, A. Smith, S. Rao, R. Twesten, S. Chaieb, M. H. Nayfeh, L. Wagner, and L. Mitas, Phys. Lett. **80**, 841 (2002).
[16] L. Mitas, J. Therrien, R. Twesten, G. Belomoin, and M. H. Nayfeh, Appl. Phys. Lett. **78**, 1918 (2001).
[17] G. Nayfeh, C. Delerue, and M. Lannoo, Phys. Rev. Lett. **76**, 2961 (1996).
[18] E. Draeger, A.J. Grossman, A. Williamson, and G. Galli, Phys. Rev. Lett. **90**, 167402 (2003).
[19] A. E. Martell and R. D. Hancock, *Metal Complexes in Aqueous Solutions* (Plenum Press, New York, 1996).
[20] G. G. Nunes, R. C. R. Bottini, D. M. Reis, P. H. C. Camargo, D. J. Evans, P. B. Hitchcock, G. Jeffery Leigh, E. L. Sá, and J. F. Soares, Inorg. Chim. Acta **357**(4), 1219 (2004).
[21] S. Rao, J. Sutin, R. Clegg, E. Gratton, M. H. Nayfeh, S. Habbal, A. Tsolakidis and R. M. Martin, Phys. Rev. B **69**, 205319 (2004).
[22] M. Dole, L. L. Mack, R. L. Hines, R. C. Mobley, L. D. Ferguson, and M. B. Alice, J. Chem. Phys. **49**, 2240 (1968).

© Author(s) 2020

[23]B. A. Thomson and J. V. Iribarne, J. Chem. Phys. **71**, 4451 (1979).
[24]Lord Rayleigh, Philos. Mag. **14**, 184 (1882).
[25]P. Kebarle and L. Tang, Anal. Chem. **65**, 972A (1993).
[26]L. Tang and P. Kebarle, Anal. Chem. **65**, 3654 (1993).
[27]P. Kebarle, J. Mass Spectrom. **35**, 804 (2000).
[28]T. Hoang, M. Stupca, K. Mantey, Y. Maximenko, N. Elhalawany, C. Carr, H. Yu, M. H. Nayfeh, and H. Morgan, "Complex of heavy magnetic ions and luminescent silicon nanoparticles," J. Appl. Phys. **114**, 164319 (2013).
[29]T. Hoang, "Complex of heavy magnetic ions and luminescent silicon nanoparticles," Ph.D. dissertation (University of Illinois at Urbana-Champaign, 2014); available at http://hdl.handle.net/2142/49361.
[30]C. Harel and A. Salin, J. Phys. B: At. Mol. Phys. **10**, 3511 (1977).
[31]Turbomole V6.3, 2011, a development of University of Karlsruhe and Forschungszentrum Karlsruhe GmbH, Turbomole GmbH, since 2007; available from http://www.turbomole.com, 1989-2007.
[32]F. Weigend and R. Ahlrichs, Phys. Chem. Chem. Phys. **7**, 3297 (2005).
[33]F. Weigend, M. Häser, H. Patzelt, and R. Ahlrichs, Chem. Phys. Lett. **294**, 143 (1998).
[34]A. Schäfer, C. Huber, and R. Ahlrichs, J. Chem. Phys. **100**, 5829 (1994).
[35]J. Tomasi, B. Mennucci, and R. Cammi, Chem. Rev. **105**(8), 2999 (2005).
[36]A. Klamt and G. Schüürmann, J. Chem. Soc., Perkin Trans. 2 **2**(5), 799 (1993).

© Author(s) 2020